GSA Data Repository Item 2019070

Lei Wu, Xiubin Lin, Eric Cowgill, Ancheng Xiao, Xiaogan Cheng, Hanlin Chen, Haifeng Zhao, Ya Shen, and Shufeng Yang, 2019, Middle Miocene reorganization of the Altyn Tagh fault system, northern Tibetan Plateau: GSA Bulletin, https://doi.org/10.1130/B31875.1.

Data Repository

The supplementary material contains:

1. A text file describing the methods used to:
    1). determine the average late Quaternary slip rate for the Altyn Tagh fault west of 94.5°E;
    2). convert seismic reflection data from the time domain to the depth domain;
    3). interpolate the age of the boundary between Stages *I* and *II*;
2. Supplementary figures:
    4). Figure S1: Probability density curves of slip rates for the Altyn Tagh Fault
    5). Figure S2: Time-depth relationship obtained from borehole P-wave logging.
    6). Figure S3: Determination of the age of the boundary between Stages I and II.
    7). Figure S4: Incremental strain rate using young age model.
3. Supplementary data tables:
    8). Table S1: Compilation of Late Quaternary slip rates for the Altyn Tagh Fault.
    9). Table S2: Chronostratigaphy of Cenozoic Strata in the Qaidam Basin.
    10). Table S3: N-S Horizontal length, incremental shortening and horizontal strain rates (Old Age Model).
    11). Table S4: Cumulative basement throw, Incremental throw, and vertical strain rates (Old Model).
    12). Table S5: N-S Horizontal length, incremental shortening and horizontal strain rates (Young Age Model).
    13). Table S6: Cumulative basement throw, Incremental throw, and vertical strain rates (Young Age Model).

1. Methods

1). Method used to determine an average late Quaternary slip rate along the Altyn Tagh fault west of 94.5 °E

Here we determine an average late Quaternary slip rate (10.0 ± 4.6 mm, 1σ) along the Altyn Tagh fault system west of 94.5 °E based on theory of normal distribution. The method we used to determine this value used the following steps.

(a) Compile reported estimates of late Quaternary slip rates along the Altyn Tagh fault system (Table S1).

(b) Assume that the rates are mean values with 1σ errors that follow a normal distribution and construct a probability density curve for each estimate west of 94.5 °E (colored curves in Fig. S1).

(c) Stack the individual probability density curves to obtain a stacked probability curve (solid black curve in Fig. S1). Although the stacked probability curve has multiple peaks, it approximates a normal distribution with a mean value of 10.0 mm/a and a 1σ error of 4.6 mm/a.

2). Method used to convert the seismic reflection data from the time domain to the depth domain

Because seismic velocities vary by unit and the degree to which the Cenozoic units are buried varies greatly in the study area, use of a simple time-depth relationship to convert the seismic reflection data from the time domain to the depth domain will introduce errors in depth location. To solve this problem, we use the **Horizon Velocity Method**, which assumes that the velocity of each unit remains the same at all depths. In this method, $\boldsymbol{Z}$ (the thickness of the layer in meters) is a function of $\boldsymbol{V}$ (the velocity of material at a given horizon) and $\boldsymbol{k}$ (rate of change of velocity within the layer):

$$Z = V_0(e^{kt} - 1)/k \qquad (1)$$

Where:

$\boldsymbol{V_0}$ is the velocity at the top of the layer in meters per second

k is the rate of change in velocity with increasing depth

t is the one way travel time for layer thickness, in seconds

If ***k*** is set to zero then ***V*** becomes an interval velocity, applying a constant velocity to each layer, i.e., $\boldsymbol{Z=V_0*t}$.

In this paper, we use a time-depth relationship obtained from borehole P-wave loggings (Fig. S2) to fit optimal parameters of $\boldsymbol{V_0}$ and ***k*** for each Cenozoic layer, and then convert the seismic reflection profiles from time domain to depth domain based on equation (1), above. Once parameters of $\boldsymbol{V_0}$ and ***k*** for each Cenozoic layer are given, the conversion is easily implemented using 2D Move software.

3). Method used to determine the age of the boundary between Stages *I* and *II*

We approximate the age of the boundary between *Stages I* and *II* (***t0)***, based on two general assumptions:

(1) The horizontal strain rates during *Stage I* remained nearly constant, which is supported by our finding that all strain rates between ~53.5 – 23 Ma during *Stage I* are within the same order of magnitude (Fig. 12).

(2) The unconformity at the base of the SY formation formed mainly during *Stage II* by intense uplift late in the period during which the the XY formation was deposited, as shown in the forward modeling (Fig. 8) and the restored sections (Figs. 9 – 11). This assumption implies that the average strain rate during *Stage I* should be lower than that during *Stage II*.

The stratigraphic data indicate the value for ***t0*** is between 23 Ma and 15.3 Ma. To identify the age of the boundary we wrote a simple C program to try every possible value of ***t0*** with a step of 0.1 million years. For each value of ***t0***, we calculate the average strain rate (*avSR*) and the corresponding total standard deviation (*Sd*) in *Stage I* (between 53.5 Ma and ***t0***). The optimal value of ***t0*** should meet two requirements corresponding to the above two assumptions: (1) the *Sd* is a minimum, and (2) the *avSR* is smaller than the averaged strain rate of the corresponding *Stage II*. Fig. S3a shows a plot of calculated *Sd* against all the possible values of ***t0***. It is clear that the smallest *Sd* is at 2.83×10^{-17} s^{-1}, which corresponds to a ***t0*** of 16.9 Ma. We use

this age for the boundary time between *Stages I* and *II* but note that this, is not an independently observed value for ***t0***, but rather the mathematically optimal value based on the two geological assumptions stated above.

In Fig. S3b we show the way we calculate the average strain rate (*avSR*) and standard deviation (*Sd*). We did not use the simple arithmetic mean of all the strain rate values as the average, because these values have different weights owing to their different effective times. Instead, we first calculated the sum of all strain rates multiplied by their corresponding effective time, and then obtained the *avSR* through dividing the sum by the total time span of *Stage I*. The way to calculate the standard deviation (*Sd*) is similar (Fig. S3b).

2. Supplementary figures

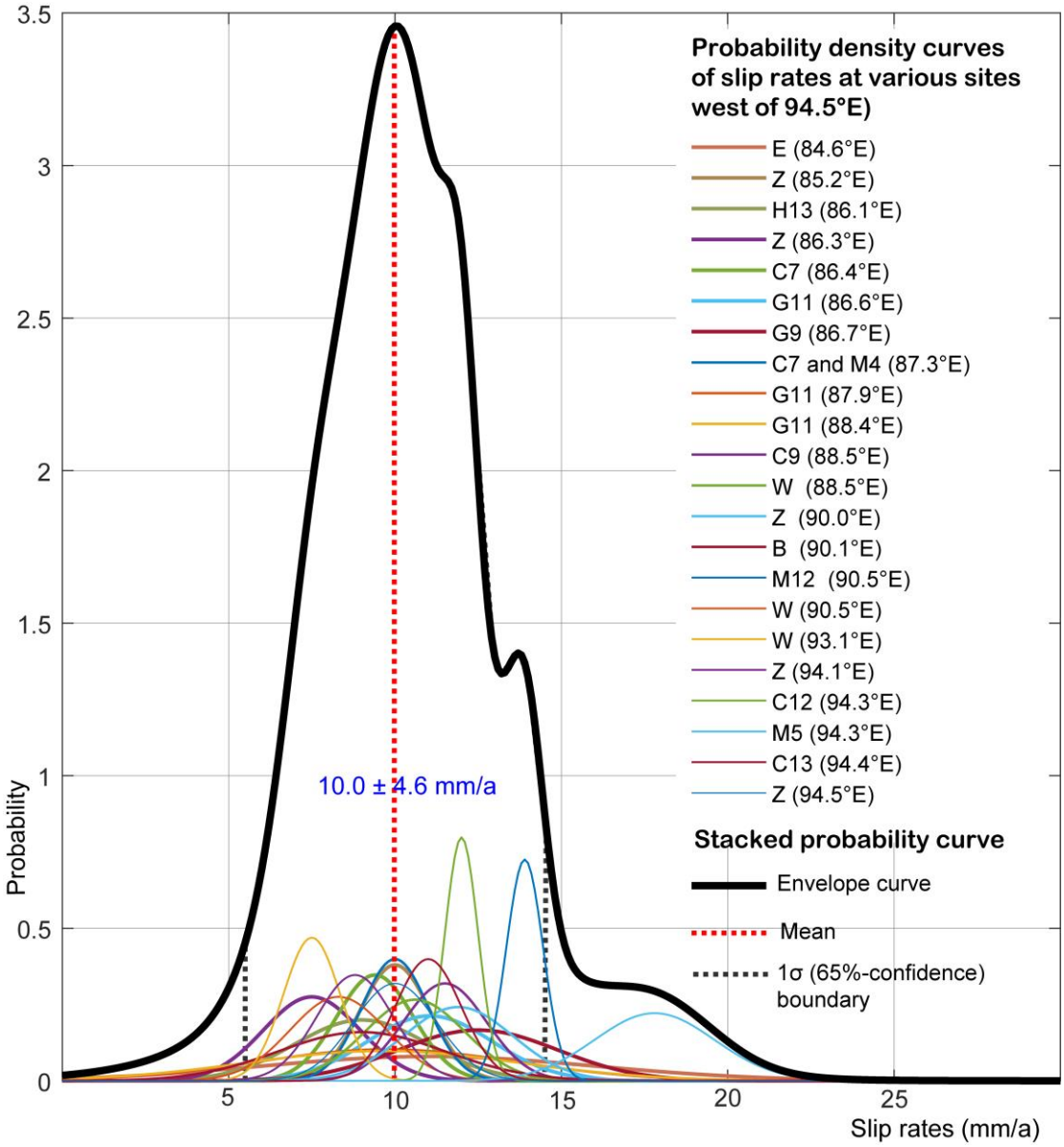

Figure S1 Probability density curves of individual slip rates (colored lines) from sites west of 94.5 ℮ and a stacked probability curve (solid black line). See Table S1 for data.

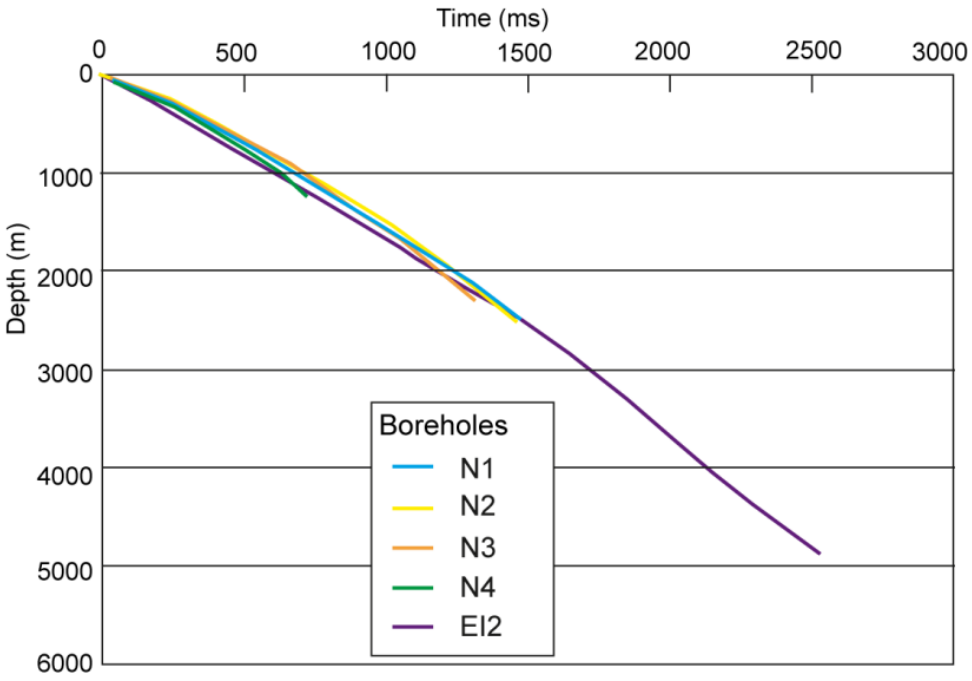

Figure S2. Time-depth relationship obtained from 5 borehole P-wave loggings within in the study area; see Fig. 2 for well locations. Depths are reported relative to the surface elevation at each borehole location.

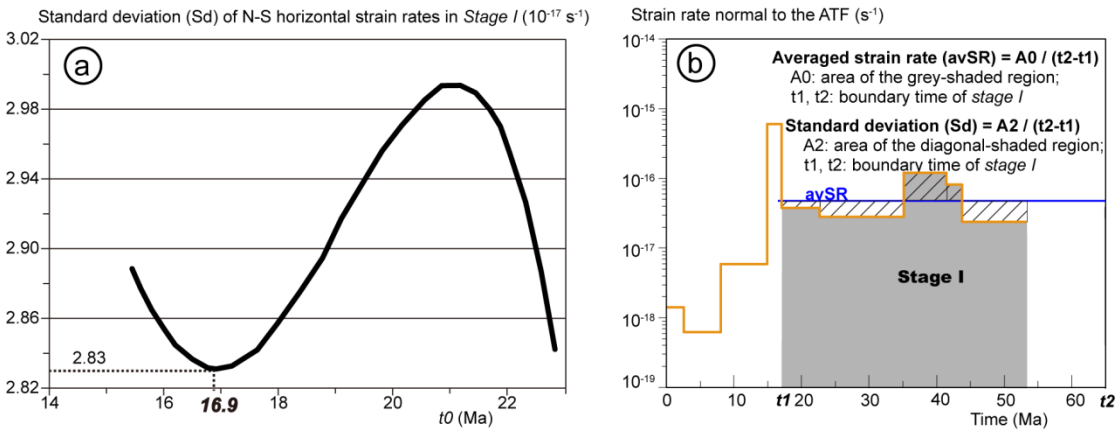

Figure S3. (a) Plot of calculated *Sd* against all the possible values of ***t0***. We use the value of ***t0*** with the smallest *Sd* as the optimal one (16.9 Ma). **(b)** The way to calculate the average strain rate (*avSR*) and standard deviation (*Sd*), which takes into account the effective time of each strain rate.

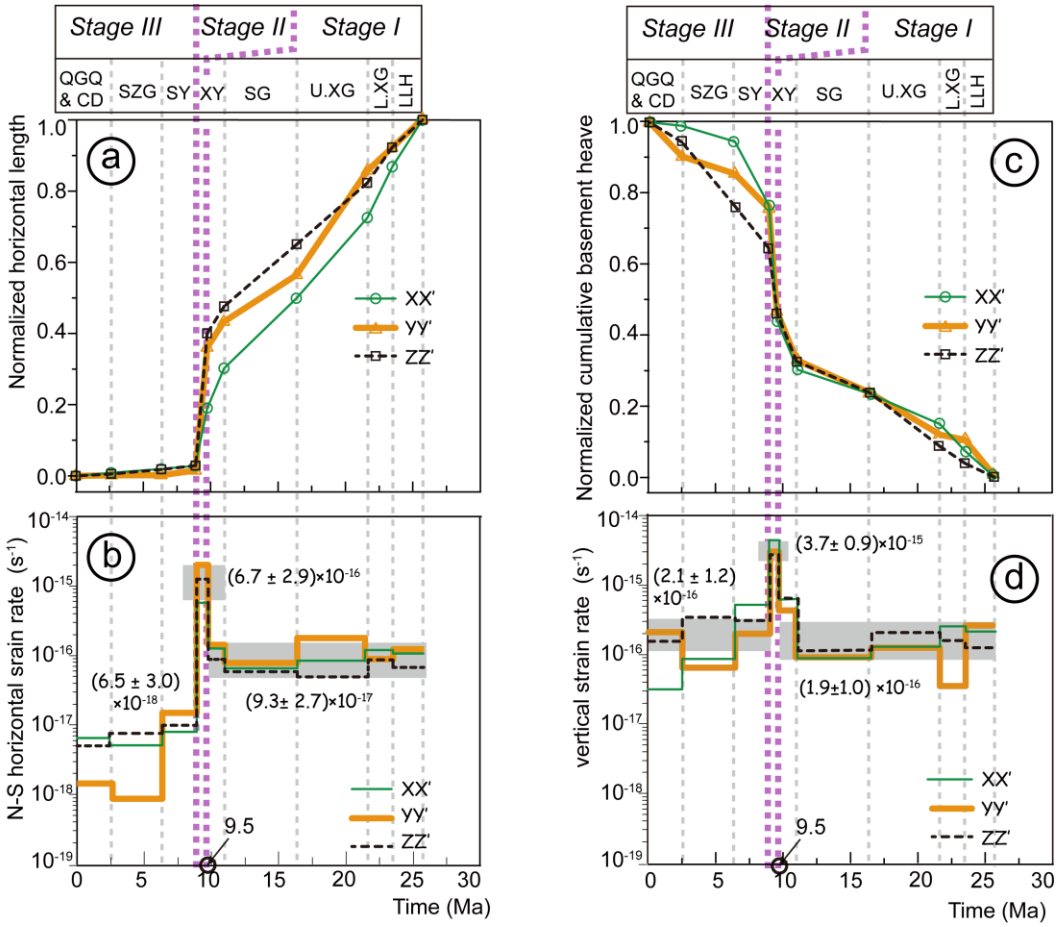

Figure S4. Plots of deformation intensity over time using young age model (Table S2). (a) N-S horizontal section length (normalized by initial section length) vs. time (present is 0 Ma); (b) N-S horizontal strain rate vs. time; (c) cumulative basement throw (normalized by total throw) vs. time; (d) vertical strain rate vs. time. Detailed data used to generate these plots are listed in Tables S5 and S6 in the Supplementary Information

3. Supplementary tables

Table S1 Summary of reported estimates of late Quaternary slip rates along the Altyn Tagh fault system, which are also shown in Fig. 1b.

Symbol	mean slip rate (mm/a)	1σ (mm/a)	2σ (mm/a)	Time scale	Reference
Z-1	<20.00mm			decadal	Zhang et al. (2007)
Data used to calculate the mean slip rate west of 94.5 °E:					
E (84.6 °E)	11	5	10	decadal	Elliott et al. (2008)
Z (85.2 °E)	10	1.05	2.1	7.9 ± 0.6 ka	Zhang et al. (2007)
H13 (86.1 °E)	9	2	4	decadal	He et al. (2013)
Z (86.3 °E)	7.5	1.45	2.9	15.3 ± 4.2 ka	Zhang et al. (2007)
C7 (86.4 °E)	9.4	1.15	2.3	16.6 ± 3.9 ka	Cowgill (2007)
G11 (86.6 °E)	11.05	1.88	3.75	6.2 - 6.1 ka	Gold et al. (2011)
G9 (86.7 °E)	12.5	2.4	4.8	6.0 ± 0.8 ka	Gold et al. (2009)
C7 & M4 (87.3 °E)	10	1	2	< 350.0 ka	Cowgill (2007) and Mériaux et al. (2004)
G11 (87.9 °E)	9.75	3.88	7.75	< 24.2 ka	Gold et al. (2011)
G11 (88.4 °E)	9.65	4.08	8.15	17.1 - 2.2 ka	Gold et al. (2011)
C9 (88.5 °E)	11.5	1.25	2.5	4.0 - 6.0 ka	Cowgill et al. (2009)
W (88.5 °E)	10.6	1.5	3	4.7 ± 0.4 ka	Wang et al. (2004)
Z (90.0 °E)	11.9	1.65	3.3	decadal	Zhang et al. (2007)
B (90.1 °E)	9	2.5	5	decadal	Bendick et al. (2000)
M12 (90.5 °E)	13.9	0.55	1.1	< 8.7 ka	Mériaux et al. (2012)
W (90.5 °E)	8.3	1.45	2.9	13.9 ± 1.1ka	Wang et al. (2004)
W (93.1 °E)	7.5	0.85	1.7	9.4 ± 0.7	Wang et al. (2004)
Z (94.1 °E)	8.8	1.15	2.3	decadal	Zhang et al. (2007)
C12 (94.3 °E)	12	0.5	1	5.8 ± 0.2 ka	Chen et al. (2012)
M5 (94.3 °E)	17.8	1.8	3.6	<14.0 ka	Mériaux et al. (2005)
C13 (94.4 °E)	11	1	2	7.4 ± 0.4 ka	Chen et al. (2013)
Z (94.5 °E)	10	1.25	2.5	4.1 ± 0.2 ka	Zhang et al. (2007)
Decreasing slip rate toward east on the Qilian segment of the Altyn Tagh fault system (east of 94.5 ° E)					
Z (94.6 °E)	7.2	0.6	1.2	~9.0 ka	Zhang et al. (2007)

Z (94.9 °E)	7	0.8	1.6	20.0 ± 2.2ka	Zhang et al. (2007)
MY (96.3 °E)	4	1	2	12.0 ± 2.0 ka	Meyer et al. (1996)
X (96.5 °E)	5.5	1	2	41.7 ± 3.3	Xu et al. (2005)
Z (96.6 °E)	3.9	1.15	2.3	decadal	Zhang et al. (2007)
X (96.7 °E)	4.2	0.5	1	28.2 ± 2.3ka	Xu et al. (2005)
S (96.8 °E)	3.75	0.48	0.95	decadal	Seong et al. (2011)
X (96.9 °E)	2.2	0.1	0.2	9.0 ± 0.7 ka	Xu et al. (2005)

Table S2 Summary of competing basal-boundary age models of the Cenozoic stratigraphy in the Qaidam Basin. Details are shown in Sections 5.6 and 5.7 and Fig. 3b.

Formation Name	Formation Abbeviation	Basal Age in Old Model (Ma)[1,2]		Basal Age in Young Model (Ma)	Basal Age Used in This Study		Reference for Age Used in This Study
		Maximum	Minimum	Wang et al. (2017)	Age (Ma)	Section on Fig. 3b	
Chaerhan-Dabuxun	CD	na	na	na	na	na	na
Qigequan	QGQ	3.2	2.5	na	2.5	A	Zhang et al., 2013
Shizigou	SZG	8.2	7.5	6.3	8.1	B2	Zhang et al., 2006
Shangyoushashan	SY	15.3	12.4	9	15.3	C	Wu, 2011
Xiayoushashan	XY	25	19.5	11.1	23	B1	Chang et al., 2015
Shangganchaigou	SG	35.5	31.5	16.5	35.5	E	Sun et al., 2005a
Upper Xiaganchaigou	UXG	na	na	na	41.5	na	interpolated (see text)
Lower Xiaganchaigou	LXG	44.2	43.8	23.5	43.8	G	Zhang, 2006
Lulehe	LLH	53.8	52	25.5	53.5	G	Zhang, 2006

[1] na: not available

[2] Ages are those assigned to the base of the formation

Table S3 N-S Horizontal length, incremental shortening, and horizontal strain rates for the three studied sections under the age constraints used in this study (old age model). Plots of these data are shown in Fig. 12*.

Formations	Lower boundary age (Ma)	N-S Horizontal Length ** (m)			Incremental horizontal shortening ** (m)			N-S horizontal strain rate*** (10^{-18} s^{-1})		
		XX'	YY'	ZZ'	XX'	YY'	ZZ'	XX'	YY'	ZZ'
/	0	32940.1±35.2	47192.2±51.2	23106.8±12.4	/	/	/	/	/	/
QGQ	2.5	32957.9±19.4	47197.6±31.7	23116.2±21.5	17.9±1.3	5.0±0.9	9.1±1.2	6.8±0.5	1.5±0.3	5.0±0.7
SZG	8.1	32980.3±79.3	47203.2±58.9	23136.1±42.1	23.1±1.7	5.1±1.1	21.2±1.8	3.9±0.3	0.7±0.1	5.1±0.5
SY	15.3	33002.9±24.5	47265.7±79.3	23153.8±33.5	23.0±1.5	62.8±3.4	17.9±1.0	3.0±0.2	5.9±0.3	3.4±0.2
XY	16.9	33332.8±36.8	48844.1±101.2	23644.8±79.8	330.5±15.7	1577.6±79.4	490.7±11.5	196.4±9.6	640.4±33.0	411.6±9.9
	23	33559.1±102.3	49182.3±198.3	23747.9±145.3	226.4±8.9	338.2±23.4	102.2±8.1	35.0±1.4	35.7±2.5	22.4±1.8
SG	35.5	33974.4±122.3	49785.8±98.3	23983.2±69.5	414.8±21.3	604.3±31.7	234.8±13.4	31.0±1.6	30.8±1.7	24.9±1.5
U. XG	41.5	34436.3±276.3	51133.2±278.5	24218.1±145.3	461.7±30.9	1346.8±97.5	235.1±15.6	70.9±4.9	139.2±10.3	51.3±3.5
L. XG	43.8	34732.2±256.8	51432.1±323.1	24351.8±275.3	296.2±18.5	299.1±31.5	135.2±7.6	117.6±7.5	80.2±8.7	76.4±4.4
LLH	53.5	35003.7±145.3	51794.9±169.4	24460.1±241.1	271.8±21.4	362.9±35.6	107.1±6.3	25.4±2.1	22.9±2.3	14.3±0.9

* The horoizontal length, shortening, and strain rate numbers correspond to values accumulated during deposition of the formation listed in the same row (i.e., since the time of the contact at the base of that Fm)

* *Values measured directly from the restored sections; Although the N-S horizontal shortening can also be calculated from differencing the horizontal section lengths between time intervals, values reported here were measured directly from the sequentially restored sections to reduce uncertainties resulting from error propagation.

***Values calculated from N-S horizontal shortenings under the age constraints used in this study (old age model, Fig. 3b and Table S2).

Table S4 Cumulative basement throw, Incremental throw, and vertical strain rates for the three studied sections under the age constraints used in this study (old age model). Plots of these data are shown in Fig. 12*.

Formations	Lower boundary age (Ma)	Cumulative basement throw** (m)			Incremental Throw** (m)			Vertical strain rate*** (10^{-16} s^{-1})		
		XX'	YY'	ZZ'	XX'	YY'	ZZ'	XX'	YY'	ZZ'
/	0	8090.1±219.3	8060.8±150.1	4636.7±100.3	/	/	/	/	/	/
QGQ	2.5	8010.2±124.3	7287.3±223.5	4355.9±79.5	79.7±8.3	773.8±63.3	280.9±12.1	0.3±0.1	2.1±0.2	1.6±0.1
SZG	8.1	7647.9±98.5	6890.2±315.4	3404.2±159.2	362.1±41.5	397.1±41.2	951.7±83.4	0.6±0.1	0.5±0.1	2.3±0.2
SY	15.3	6186.8±122.3	6094.5±179.4	2787.4±80.5	1460.8±101.6	795.2±89.5	616.2±35.4	2.0±0.1	0.8±0.1	1.2±0.1
XY	16.9	3617.1±215.2	3747.3±168.5	1806.2±101.2	2568.7±345.2	2347.6±156.4	981.5±94.7	15.6±2.1	10.4±0.6	8.7±0.8
	23	2452.3±247.9	2668.1±198.5	1081.7±111.3	1164.7±111.3	1078.7±98.7	724.2±65.3	1.8±0.2	1.2±0.1	1.6±0.1
SG	35.5	1925.4±79.5	1916.8±154.3	625.3±214.5	527.1±36.8	751.2±54.2	456.8±32.1	0.4±0.1	0.4±0.1	0.5±0.1
U. XG	41.5	1203.6±98.4	953.1±213.5	-164.2±187.1	721.4±36.5	963.7±103.4	788.7±95.2	1.2±0.1	1.1±0.1	1.7±0.2
L. XG	43.8	595.1±59.3	832.2±154.6	-406.1±34.6	608.7±55.8	120.2±6.5	242.3±10.5	2.5±0.2	0.3±0.1	1.4±0.1
LLH	53.5	0.0±0.0	0.0±0.0	-605.8±59.1	595.2±14.3	832.2±15.2	200.1±15.6	0.6±0.1	0.5±0.1	0.3±0.1

* The cumulative basement throw, incremental throw, and vertical strain rate numbers correspond to values accumulated during deposition of the formation listed in the same row (i.e., since the time of the contact at the base of that Formation)

** Values measured directly from the restored sections; note that although the incremental throws can also be calculated from differencing the cumulative basement throw values between time intervals, values reported here were measured directly from the sequentially restored sections to reduce the uncertainties resulting from error propagation.

***Values calculated from incremental throw under the age constraints used in this study (old age model, Fig. 3b and Table S2).

Table S5 N-S Horizontal length, incremental shortening, and horizontal strain rates for the three studied sections using the young age model (Table S2). Plots of the data are shown in Fig. S4*.

Formations	Lower boundary age (Ma)	N-S Horizontal Length ** (m)			Incremental horizontal shortening ** (m)			N-S horizontal strain rate*** (10^{-18} s^{-1})		
		XX'	YY'	ZZ'	XX'	YY'	ZZ'	XX'	YY'	ZZ'
/	0	32940.1±35.2	47192.2±51.2	23106.8±12.4	/	/	/	/	/	/
QGQ	2.5	32957.9±19.4	47197.6±31.7	23116.2±21.5	17.9±1.3	5.0±0.9	9.1±1.2	6.8±0.5	1.5±0.3	5.0±0.7
SZG	6.3	32980.3±79.3	47203.2±58.9	23136.1±42.1	23.1±1.7	5.1±1.1	21.2±1.8	5.7±0.4	1.0±0.2	7.4±0.6
SY	9	33002.9±24.5	47265.7±79.3	23153.8±33.5	23.0±1.5	62.8±3.4	17.9±1.0	8.0±0.5	15.6±0.8	9.0±0.5
XY	9.5	33332.8±36.8	48844.1±101.2	23644.8±79.8	330.5±15.7	1577.6±79.4	490.7±11.5	628.6±29.9	2049.3±103.1	1317.1±30.9
	11.1	33559.1±102.3	49182.3±198.3	23747.9±145.3	226.4±8.9	338.2±23.4	102.2±8.1	133.5±5.2	136.1±9.4	85.4±6.8
SG	16.5	33974.4±122.3	49785.8±98.3	23983.2±69.5	414.8±21.3	604.3±31.7	234.8±13.4	71.7±3.7	71.2±3.7	57.5±3.3
U. XG	21.5	34436.3±276.3	51133.2±278.5	24218.1±145.3	461.7±30.9	1346.8±97.5	235.1±15.6	85.1±5.7	167.1±12.1	61.5±4.1
L. XG	23.5	34732.2±256.8	51432.1±323.1	24351.8±275.3	296.2±18.5	299.1±31.5	135.2±7.6	135.3±8.4	92.2±9.7	87.9±4.9
LLH	25.5	35003.7±145.3	51794.9±169.4	24460.1±241.1	271.8±21.4	362.9±35.6	107.1±6.3	123.1±9.7	111.0±10.9	69.4±4.1

* The horoizontal length, shortening, and strain rate numbers correspond to values accumulated during deposition of the formation listed in the same row (i.e., since the time of the contact at the base of that Fm)

** Values measured directly from the restored sections; note that although the N-S horizontal shortening can also be calculated from differencing the horizontal section lengths between time intervals, values reported here were measured directly from the sequentially restored sections to reduce uncertainties resulting from error propagation.

*** Values calculated from N-S incremental horizontal shortenings using the young age model (Table S2)

Table S6 Cumulative basement throw, Incremental throw, and vertical strain rates for the three studied sections using the young age model (Table S2). Plots of the data are shown in Fig. S4*.

Formations	Lower boundary age (Ma)	Cumulative basement throw** (m)			Incremental Throw** (m)			Vertical strain rate*** (10^{-16} s^{-1})		
		XX'	YY'	ZZ'	XX'	YY'	ZZ'	XX'	YY'	ZZ'
/	0	8090.1±219.3	8060.8±150.1	4636.7±100.3	/	/	/	/	/	/
QGQ	2.5	8010.2±124.3	7287.3±223.5	4355.9±79.5	79.7±8.3	773.8±63.3	280.9±12.1	0.3±0.1	2.1±0.2	1.6±0.1
SZG	6.3	7647.9±98.5	6890.2±315.4	3404.2±159.2	362.1±41.5	397.1±41.2	951.7±83.4	0.9±0.1	0.7±0.1	3.4±0.3
SY	9	6186.8±122.3	6094.5±179.4	2787.4±80.5	1460.8±101.6	795.2±89.5	616.2±35.4	5.2±0.4	2.0±0.2	3.1±0.2
XY	9.5	3617.1±215.2	3747.3±168.5	1806.2±101.2	2568.7±345.2	2347.6±156.4	981.5±94.7	50.1±6.7	33.1±2.2	27.9±2.7
	11.1	2452.3±247.9	2668.1±198.5	1081.7±111.3	1164.7±111.3	1078.7±98.7	724.2±65.3	7.0±0.7	4.5±0.4	6.1±0.6
SG	16.5	1925.4±79.5	1916.8±154.3	625.3±214.5	527.1±36.8	751.2±54.2	456.8±32.1	1.0±0.1	0.9±0.1	1.1±0.1
U. XG	21.5	1203.6±98.4	953.1±213.5	-164.2±187.1	721.4±36.5	963.7±103.4	788.7±95.2	1.4±0.1	1.3±0.1	2.1±0.3
L. XG	23.5	595.1±59.3	832.2±154.6	-406.1±34.6	608.7±55.8	120.2±6.5	242.3±10.5	2.8±0.3	0.4±0.1	1.6±0.1
LLH	25.5	0.0±0.0	0.0±0.0	-605.8±59.1	595.2±14.3	832.2±15.2	200.1±15.6	2.7±0.1	2.6±0.1	1.3±0.1

* The cumulative basement throw, incremental throw, and vertical strain rate numbers correspond to values accumulated during deposition of the formation listed in the same row (i.e., since the time of the contact at the base of that Fm)

**Values measured directly from the restored sections; note that although the incremental throws can also be calculated from differencing the cumulative basement throw values between time intervals, values reported here were measured directly from the sequentially restored sections to reduce the uncertainties resulting from error propagation.

***Values calculated from incremental throw using the young age model (Table S2).